Materials science communication

Control of dielectric properties in bismuth ferrite multiferroic by compacting pressure

A.V. Pashchenko [a,b,c,d], N.A. Liedienov [a,b,*], Quanjun Li [a], I.I. Makoed [e], D.D. Tatarchuk [f], Y.V. Didenko [f], A.I. Gudimenko [g], V.P. Kladko [g], Lina Jiang [a], Liping Li [h], V.G. Pogrebnyak [d], G.G. Levchenko [a,b,**]

[a] State Key Laboratory of Superhard Materials, International Center of Future Science, Jilin University, 130012, Changchun, China
[b] Donetsk Institute for Physics and Engineering Named After O. O. Galkin, NASU, 03028, Kyiv, Ukraine
[c] Institute of Magnetism NASU and MESU, 03142, Kyiv, Ukraine
[d] Ivano-Frankivsk National Technical University of Oil and Gas, MESU, 76019, Ivano-Frankivsk, Ukraine
[e] A. S. Pushkin Brest State University, 224016, Brest, Belarus
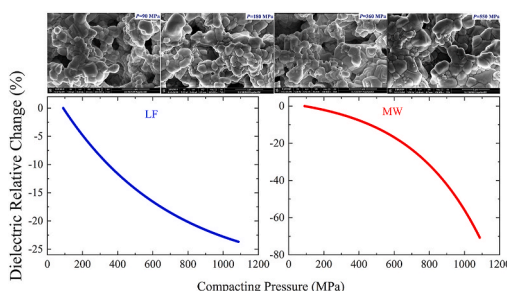[f] National Technical University of Ukraine "Igor Sikorsky KPI", 03056, Kyiv, Ukraine
[g] V.E. Lashkaryov Institute of Semiconductor Physics, NASU, 03028, Kyiv, Ukraine
[h] State Key Laboratory of Inorganic Synthesis and Preparative Chemistry, College of Chemistry, Jilin University, 130012, Changchun, PR China

HIGHLIGHTS

- Single-phase BLFO ceramics were synthesized by RLS method under different pressures.
- Optimal conditions for formation of BLFO perovskite are 850 °C after 5 min in air.
- Compacting pressure can change ε' of BLFO by ~25% in LF and by ~80% in MW ranges.

GRAPHICAL ABSTRACT

ARTICLE INFO

ABSTRACT

Single-phase lanthanum-modified bismuth ferrite multiferroic ceramics have been synthesized by the rapid liquid-phase sintering (RLS) method. Phase composition, crystal structure, microstructure and dielectric properties of the $Bi_{0.9}La_{0.1}FeO_3$ multiferroic have been studied using TG/DTA, XRD, SEM, capacitive and composite dielectric resonator methods. It has been established that the optimal conditions for formation of a perovskite $Bi_{0.9}La_{0.1}FeO_3$ structure are 850 °C after 5 min in air. It has been found that the compacting pressure of the initial mixture of precursors from 90 to 1090 MPa can change the dielectric constant by ~25% in the low-frequency range and by ~80% in the microwave range up to complete elimination of the elastic polarization mechanism. The use of the RLS method under various compacting pressures opens additional possibilities for creating multifunctional multiferroics with controlled magnetoelectric coupling.

---

1. Introduction

Metal oxides based on bismuth ferrite $BiFeO_3$ with a perovskite structure belong to the class of multiferroics – the multifunctional materials where there are two or more types of ferro-ordered states [1–3]. The coexistence of magnetostrictive and piezoelectric properties is the reason for the appearance of the magnetoelectric (ME) effect [4,5]. Nowadays, the ME effect has found application in supersensitive sensors of alternating and constant magnetic field [6]. Based on the ME effect, it is possible to create high-precision microwave equipment [7] and miniature electronic devices for wireless energy transfer [8]. Multiferroics are used to reduce the electrical noise in ME sensors [9]. Multilayer film heterostructures based on bismuth ferrite have a high potential for use in high-speed memory devices with low energy consumption and high memory density [10]. ME laminate composite configurations are also used in non-invasive neurological interfaces [11,12]. Despite extensive study of multiferroic bismuth ferrite, the relevance of this research remains, since this material is the only non-composite Type-I single-phase multiferroic that has high temperatures of the appearance of magnetoelectric coupling [13].

The appearance of a colossal linear ME effect is observed when bismuth is replaced by lanthanum in bulk $BiFeO_3$ material [14]. One of the advantages of $Bi_{0.9}La_{0.1}FeO_3$ composition is the high values of the dielectric constant ε' [15,16]. However, the synthesis of single-phase bismuth ferrite with a perovskite structure is quite complex task [17, 18]. The appearance of $Bi_{25}FeO_{40}$ and $Bi_2Fe_4O_9$ minor phases leads to a leakage current and degrade the functional properties of multiferroics. It is appropriate to synthesize single-phase bismuth ferrite by the rapid liquid-phase sintering (RLS) method [16], since the minor phases of $Bi_{25}FeO_{40}$ and $Bi_2Fe_4O_9$ do not have time to form due to a rapid heating and cooling initial mixture of precursors. Using RLS method to synthesize $Bi_{0.9}La_{0.1}FeO_3$ ceramics, it has been found that the compacting pressure P of the initial powder mixture affects the dielectric properties of multiferroic [15,19]. However, these studies were conducted in a narrow range of pressure and frequency. The search for new mechanisms in order to control of ME coupling in a wider frequency range is a topical task to increase the functionality of multiferroics. Therefore, to expand the possibilities of using $Bi_{0.9}La_{0.1}FeO_3$ ceramics, it becomes important to increase the range of pressure and frequency variation which is the main goal of this work.

2. Experimental

Ceramic samples of $Bi_{0.9}La_{0.1}FeO_3$ were obtained by the RLS method [16]. The initial La_2O_3 (purity $\geq$ 99.9% from Aladdin), Bi_2O_3 (purity $\geq$ 99.9% from Aladdin), and Fe_2O_3 (purity $\geq$ 99.5% from Aladdin) powders were mixed in a stoichiometric ratio and pressed into tablets with a diameter of ¼" (6.35 mm) under compacting pressure P = 90, 180, 360, 545, 725, 900, and 1090 MPa with an accuracy of ±9 MPa. The compacted samples were sintered in air at a temperature of t_{ann} = 850°C for a short time 480 s. As a result, the BLFO-90, BLFO-180, BLFO-360, BLFO-545, BLFO-725, BLFO-900, and BLFO-1090 samples with different compacting pressures P of precursors from 90 to 1090 MPa were obtained. It should be noted that the choice of the environment atmosphere for sintering process in the RLS method is an important task due to possible influence on the chemical composition, microstructure, porosity and properties of the material [20]. Synthesis of bismuth ferrite in N_2 atmosphere in comparison with O_2 leads to an improvement in the crystallization characteristics and to a decrease in the content of minor $Bi_2Fe_4O_9$ and $Bi_{25}FeO_{40}$ phases [18]. However, N_2 gas in the pores prevents complete compaction of the grains and can lead to swelling of the sample with a simultaneous loss of material properties. Therefore, the synthesis of BLFO ceramics was carried out in air with ~21% oxygen and ~78% nitrogen.

The phase formation processes in the system Bi_2O_3–La_2O_3–Fe_2O_3 was studied by simultaneous thermogravimetry/differential thermal analysis (TG/DTA) using Linseis STA PT 1600. The TG/DTA curves were recorded in the range of 25–900 °C with a heating rate of 30 °C min^{-1}. The initial precursor mixture mass was about 22 mg and weighed to alumina crucibles. The experiments were carried out in air at a flow rate of 100 mL min^{-1}. The reference substance was pure α-Al_2O_3. Symmetry, crystal lattice parameters, and phase composition were determined using a high-resolution PANalitical X-Pert PRO MRD diffractometer in $Cu_{K\alpha1}$ radiation. The diffraction reflection patterns were recorded in the 2 theta-omega mode (scanning pitch of 0.02°, time at a point of 2 s). Lattice parameters were determined with an accuracy ±0.001 Å. Qualitative phase analysis was performed using the ICDD database, PDF-2 Release 2012, and the Crystallographica Search-Match program Version 3, 1, 0, 0. The concentrations of the phases present were found by the corundum number method [21]. The microstructure, crystallite size, and chemical composition refinement were determined by scanning electron microscopy (SEM) on a FEI MAGELLAN 400 Scanning Electron Microscope. The survey was carried out in a high vacuum mode using a "through-lens" (TLD) detector at an accelerating voltages of 5–10 kV and high beam currents of 0.20–0.40 nA with magnification up to 65 000 X. The size of grains was determined from analysis of SEM images within clear and defined grain boundaries using Nano Measure 1.2.5 software [22]. The dielectric properties were studied by analyzing the frequency dependences of the dielectric constant $\varepsilon'(f)$ and the dielectric loss tangent $\tan\delta(f)$ at room temperature in the low-frequency (LF) range from 0.1 to 10^6 Hz by the capacitive method and in the microwave (MW) range from 8 to 12 GHz by the composite dielectric resonator method [23]. An accuracy of determination of $\varepsilon'(f)$ and $\tan\delta(f)$ does not exceed 3 and 5% for LF, and 5 and 15% for MW ranges, respectively. The $\varepsilon'(f)$ and $\tan\delta(f)$ measurements in the LF range [16] were carried out using graphite powder rubbed homogeneously over the entire surface on both sides of the cylindrical samples (d = 6.35 mm and h = 2–3 mm).

3. Results and discussion

According to the TG/DTA studies for the stoichiometric Bi_2O_3–La_2O_3–Fe_2O_3 mixture of precursors (see Supplementary Material), an exothermic effect is observed near 850 °C that is associated with the crystallization process of the perovskite multiferroic phase [24]. At stabilized temperature of 850 °C, an exothermic peak appears after ~5 min without loss of sample mass. Therefore, the optimal conditions for obtaining single-phase multiferroics were chosen 850 °C during ~8 ≥ 5 min that was also noted in our previous work for the same composition [16].

According to X-ray diffraction data (see Fig. 1), the phase composition of the initial mixture of Bi_2O_3, La_2O_3, and Fe_2O_3 precursors before synthesis corresponds to the stoichiometric BLFO composition. After synthesis, all BLFO samples become single-phase ones and crystallize into the hexagonal $R3c$ (ICDD: 98-001-5299) perovskite structure. The compacting pressure P does not affect the symmetry and lattice parameters of the crystal structure, which slightly deviate from the unit cell parameters of a = 5.573 Å and c = 13.878 Å for BLFO-90.

The results of SEM studies confirmed the phase, chemical, and stoichiometric compositions for all BLFO samples, which are also independent of pressure P (see Fig. 2). The average crystallite size D is in the range from 200 to 300 nm and weakly depends on P. Despite the short synthesis time (8 min), all samples demonstrate a well-formed microstructure with clear boundaries of intergranular zones.

The dispersion of the dielectric permittivity components has a relaxation character (see Fig. 3). In the LF range, with an increase in the pressure P from 90 to 725 MPa, the constant ε' decreases by ~1.2 times, i.e. ~ −25% (see Fig. 4(a)). With a further increase in P from 725 to 1090 MPa, the constant ε' becomes independent of pressure P. In the LF range, small dielectric losses $\tan\delta < 1$ slightly depend on P. The $\tan\delta(f)$ dependences show two minima in the ranges from 1 to 10 Hz and from 10^4 to 10^5 Hz (see Fig. 3(b)). The appearance of these minima is
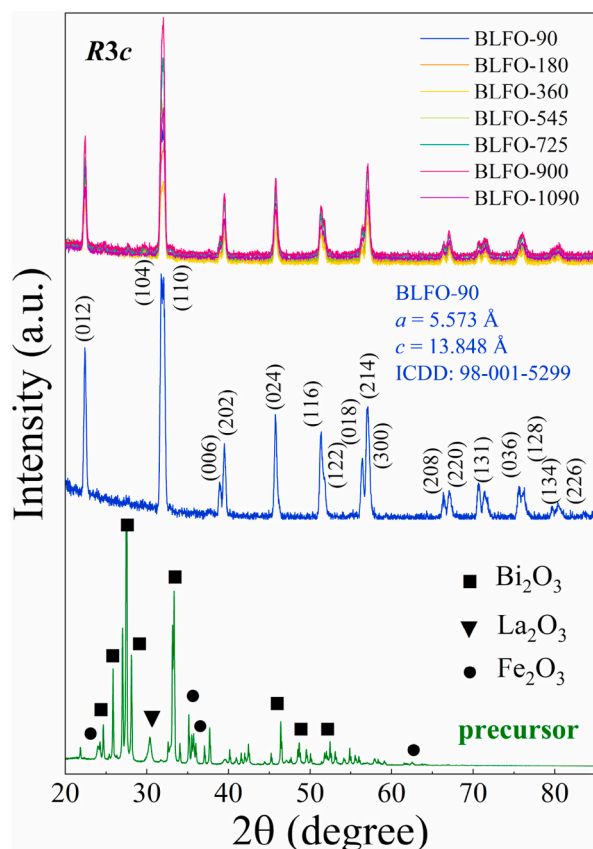
Fig. 1. Evolution of the diffraction patterns for BLFO ceramics with increase in compacting pressure *P* from 90 to 1090 MPa and the diffraction pattern for the initial mixture of precursors.

associated with the coexistence of migration and hopping polarizations in these frequency ranges [25].

The main mechanisms of dielectric polarization in the bismuth ferrite multiferroic within the LF range are hopping charge transfer between different valence Fe^{3+} and Fe^{2+} ions, and intergranular polarization associated with accumulation of weakly bound charge carriers on structural inhomogeneities, grain boundaries, and point defects [16, 26,27]. An additional contribution to the dielectric constant can be made by the high conductivity of the samples. A characteristic feature of samples with high conductivity is the presence of large losses tanδ ~1 [28–30]. The small losses tanδ ~0.03 at LF of ~1 Hz in BLFO ceramics (see Fig. 4(b)) indicate a weak contribution to the polarization effects from the conducting subsystem. The appearance of colossal values of the dielectric constant ε' ~10^5 in the lanthanum-modified bismuth ferrite multiferroics is due to the contribution high conductivity to ε' [16]. In our case, the temperature RLS regime was strictly performed in order to exclude the appearance of different valence iron ions, which are responsible for high conductivity.

The appearance of two minima in the tanδ(*f*) dependences (see Fig. 3 (b)) is due to the coexistence of various relaxation processes associated with the migration of quasi-free charge carriers. The first minimum in the range 1–10 Hz corresponds to grain-boundary effects with the localization of weakly bound charge carriers at grain boundaries (crystallites), and the second minimum in the range 10^4–10^5 Hz corresponds to localization of charge carriers on non-stoichiometry defects inside grains [31,32]. With a decrease in the frequency of *f* < 10^6 Hz, the processes associated with electron hopping between different valence iron cations reach saturation, which leads to the constant value of tanδ. However, below the frequency of *f* ≤ 10^4 Hz, quasi-free carriers begin to localize at defects inside grains. The number of quasi-free charge

carriers, which respond to a change in the sign of the external electric field, increases that leads to an increase in the dielectric loss tangent [15]. The appearance of LF minimum tanδ with a sharp increase in the loss tangent at *f* < 2 Hz is the result of the inclusion of another polarization mechanism, which is associated with charge accumulation at grain boundaries. The length of the intergranular zones and the concentration of localized charge carriers increase with a decrease in grain size. Since the pressure *P* almost does not affect the crystallite size (see Fig. 2), this polarization mechanism requires a more detailed analysis to determine the reasons for the increase in ε' with a decrease in *P* (see Figs. 3(a) and 4(a)).

The effect of pressure *P* on the dielectric constant ε' in the LF range is due to the feature of RLS method for the synthesis of BLFO ceramics. The liquid-phase sintering is often used as a compaction process in the production of various ceramic components [33]. Sintering under pressure increases the density of ceramics and makes the microstructure more uniform. After relieving the compacting pressure, the residual stress enhances the driving forces for densification in all stages of the liquid-phase sintering. The liquid phase fills the pores and small capillaries between solid particles [34]. In liquid-phase sintering, the compaction of the microstructure occurs due to a decrease in the porosity of the grains at the boundary of the intergranular zones [35]. Therefore, an increase in the compacting pressure *P* during the RLS causes a decrease in microstructural defects at the grain boundaries of BLFO where charge accumulation occurs. A decrease in the charge concentration at the grain boundaries is associated with a decrease in ε' in the range from 0.1 to 10 Hz with an increase in the compacting pressure from *P* = 90–725 MPa (see Fig. 3(a)). The absence of the influence of *P* on ε' in the range of *P* = 725–1090 MPa is due to the saturation of microstresses. While synthesis of samples at *P* > 725 MPa, due to a significant increase in microstresses, the piston is ejected from the mold after relieving the *P*.

The nature of dielectric polarization in the frequency range from 10^7 to 10^9 Hz is not fully understood. The most probable mechanism of dielectric polarization in this frequency range is the motion of the ferroelectric domain walls [36]. With increase in frequency of the external electric field and due to the large inertia, mechanisms associated with migration and hopping polarizations are eliminated. In the MW range, the main polarization mechanisms are elastic mechanisms caused by the oscillation of domain walls [37], as well as ionic and electronic polarizabilities [38–40].

In the MW range, the dielectric constant ε' and the losses tanδ are independent of the frequency for all pressures *P* (see Fig. 3). In this frequency range, the *P* strongly affects the dielectric constant, which decreases from ε' = 7.0 for 90 MPa to 2.2 for 1090 MPa (see Fig. 4(c)). The tanδ = 0.0009–0.0013 is independent of the *P* and retains its value within the experimental error (see Fig. 4(d)). The influence of the *P* on the constant ε' in the MW range is also related to the features of the RLS method. In the polycrystalline bismuth ferrite multiferroic, the size of the ferroelectric domains is in the nanometer range and coincides with the grain size [41]. As it was noted above, an increase in the *P* leads to a decrease in the concentration of charge carriers which accumulate at grain boundaries. Consequently, at elastic oscillation of the domain walls, a decrease in the charge concentration at the domain boundaries will be accompanied by a decrease in the dielectric constant ε'. As it follows from the analysis of experimental data, with an increase in the *P* to 1090 MPa, the dielectric constant decreases to ε' = 2.2. Such a small value of the dielectric constant can correspond to the contribution only from the ionic and electronic elastic polarizations. Therefore, the compacting pressure at liquid-phase synthesis can control the elastic polarization caused by the oscillation of the ferroelectric domain walls up to the complete elimination of this mechanism. Varying pressure value, the conductivity of the domain walls can be controlled. The bound charge on such domain walls can lead to a local dielectric-metal transition [42] and to a strong increase in the dielectric and piezoelectric properties [43]. The ability to control the dielectric properties of multiferroics

opens up new prospects for the practical use of the RLS method in creating new materials for nanoelectronic devices of the future.

4. Conclusions

The single-phase lanthanum-modified bismuth ferrite $Bi_{0.9}La_{0.1}FeO_3$ ceramics have been synthesized by the rapid liquid-phase sintering method at various compacting pressures of the stoichiometric mixture of precursors from 90 to 1090 MPa. It has been found out that a perovskite formation begins at ~5 min upon an optimum sintering temperature of 850 °C in air.

In the low-frequency range the dielectric constant has a relaxation behavior that is due to the thermally activated polarization mechanism. The synthesized ceramics have low dielectric losses because of the small
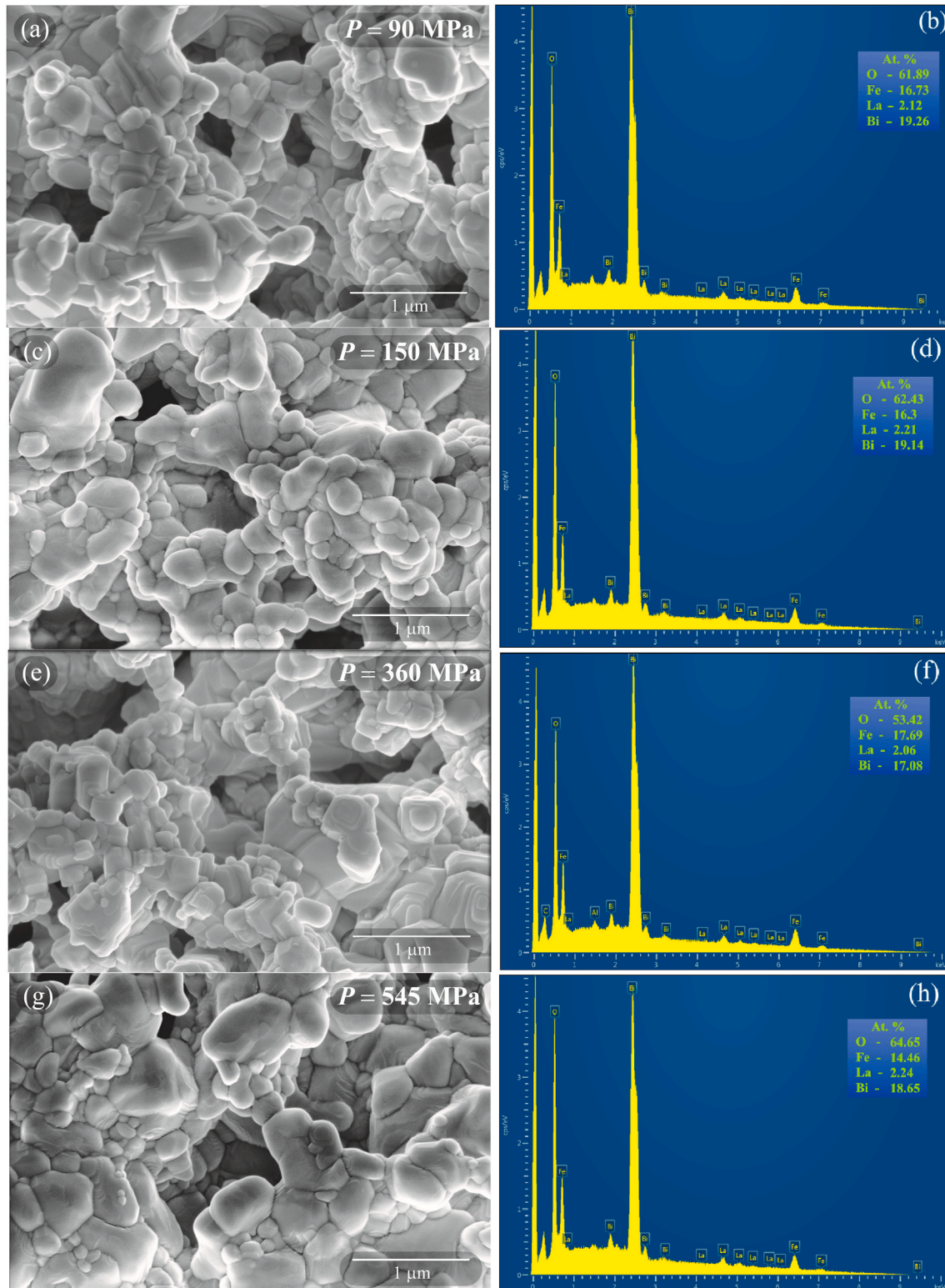

Fig. 2. SEM images (a, c, e, g) and EDS spectra (b, d, f, h) for the $Bi_{0.9}La_{0.1}FeO_3$ ceramics obtained at various compacting pressure *P*.
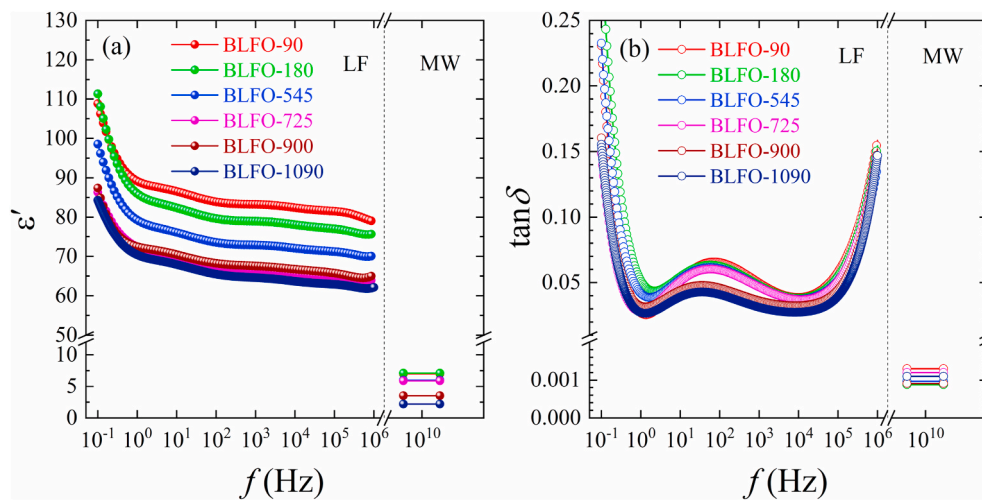
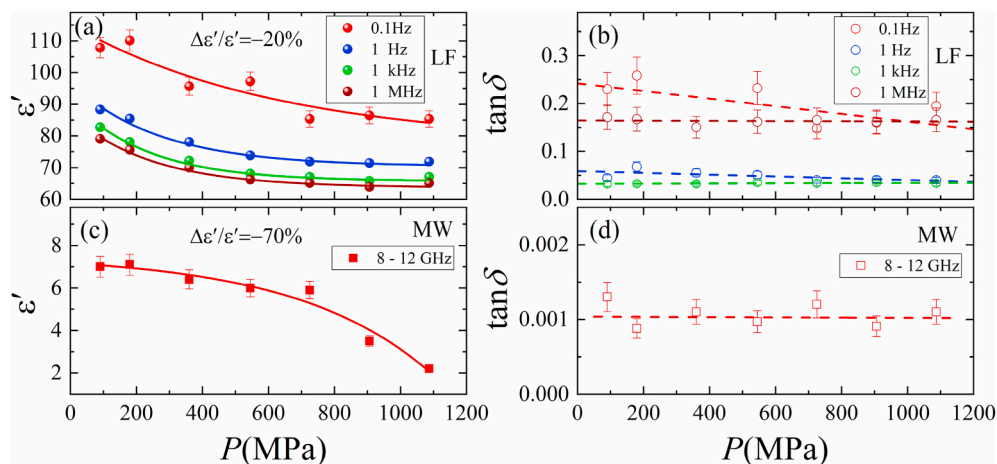**Fig. 3.** The ε′(*f*) (a) and tanδ(*f*) (b) dependences for the BLFO ceramics in the LF and MW ranges.

Fig. 4. The effect of compacting pressure *P* on the dielectric properties of BLFO multiferroics in the LF and MW ranges. The dashed line shows a linear approximation.

contribution to the dielectric polarization from migration conductivity. The strong dependence of the constant ε′ on pressure *P* in the LF range is due to the features of the rapid liquid-phase sintering method, where the pressure *P* affects the filling of pores and small capillaries between solid particles by the liquid phase. A decrease in the constant ε′ with an increase in the *P* by ~25% is associated with a decrease in the number of microstructural defects at the grain boundaries where charge accumulation occurs.

In the microwave range, the strongest influence of the compacting pressure *P* on the dielectric constant ε′ by ~80% has been found. The elastic polarization mechanism, which affects the oscillation of the ferroelectric domain walls, can be controlled by the compacting pressure up to the complete elimination. The ability to control magnetoelectric coupling through a dielectric constant in multiferroics based on bismuth ferrite opens up prospects for the practical use of the rapid liquid-phase sintering method in creating new functional materials.

Credit author statement

A.V. Pashchenko: Conceptualization; Data curation; Supervision; Investigation; Roles/Writing -original draft. **N.A. Liedienov**: Data curation; Investigation; Project administration; Writing – editing. **Quanjun Li**: Formal analysis; Resources; Software; Visualization. **I.I. Makoed**: Formal analysis; Methodology; Software; Visualization. **D.D.**

Tatarchuk: Data curation; Investigation; Formal analysis; Methodology. **Y.V. Didenko**: Data curation; Investigation; Formal analysis; Methodology. **A.I. Gudimenko**: Data curation; Investigation; Formal analysis; Methodology. **V.P. Kladko**: Formal analysis; Resources; Software. **Lina Jiang**: Data curation; Investigation; Formal analysis; Methodology. **Liping Li**: Formal analysis; Software; Visualization. **V.G. Pogrebnyak**: Formal analysis; Software; Visualization. **G.G. Levchenko**: Formal analysis; Project administration; Resources; Supervision; Writing - editing.

Declaration of competing interest

The authors declare that they have no known competing financial interests or personal relationships that could have appeared to influence the work reported in this paper.

Appendix A. Supplementary data

Supplementary data to this article can be found online at https://doi.org/10.1016/j.matchemphys.2020.123925.

References

[1] W. Eerenstein, N.D. Mathur, J.F. Scott, Nature 442 (2006) 759–765, https://doi.org/10.1038/nature05023.

[2] M.M. Kumar, V.R. Palkar, K. Srinivas, S.V. Suryanarayana, Appl. Phys. Lett. 76 (2000) 2764–2766, https://doi.org/10.1063/1.126468.

[3] YuE. Roginskaya, YuA. Tomashpol'skii, YuN. Venevtsev, V.M. Petrov, G. S. Zhdanov, J. Exp. Theor. Phys. 23 (1966) 47–51.

[4] S.K. Mandal, G. Sreenivasulu, V.M. Petrov, G. Srinivasan, Phys. Rev. B 84 (2011), 014432, https://doi.org/10.1103/physrevb.84.014432.

[5] J.S. Andrew, J.D. Starr, M.A.K. Budi, Scripta Mater. 74 (2014) 38–43, https://doi.org/10.1016/j.scriptamat.2013.09.023.

[6] M.M. Vopson, Crit. Rev. Solid State Mater. Sci. 40 (2015) 223–250, https://doi.org/10.1080/10408436.2014.992584.

[7] C. Tu, Z.-Q. Chu, B. Spetzler, P. Hayes, C.-Z. Dong, X.-F. Liang, H.-H. Chen, Y.-F. He, Yu-Yi Wei, I. Lisenkov, H. Lin, Y.-H. Lin, J. McCord, F. Faupel, E. Quandt, N.-X. Sun, Materials 12 (2019) 2259, https://doi.org/10.3390/2Fma12142259.

[8] T. Rupp, B.D. Truong, S. Williams, S. Roundy, Materials 12 (2019) 512, https://doi.org/10.3390/ma12030512.

[9] Z. Chu, M.J. PourhosseiniAsl, S. Dong, J. Phys. D Appl. Phys. 51 (2018), 243001, https://doi.org/10.1088/1361-6463/aac29b.

[10] W. Huang, Y. Liu, Z. Luo, C. Hou, W. Zhao, Y. Yin, X. Li, J. Phys. D Appl. Phys. 51 (2018), 234005.

[11] J. Zhai, Z. Xing, S. Dong, J. Li, D. Viehland, Appl. Phys. Lett. 88 (2006), 062510, https://doi.org/10.1063/1.2172706.

[12] G. Mioni, S. Grondin, L. Bardi, F. Stablum, Behav. Brain Res. 377 (2020), 112232, https://doi.org/10.1016/j.bbr.2019.112232.

[13] Chengliang Lu, Menghao Wu, Lin Lin, Jun-Ming Liu, National Science Review 6 (2019) 653–668, https://doi.org/10.1093/nsr/nwz091.

[14] A.M. Kadomtseva, Y.F. Popov, A.P. Pyatakov, G.P. Vorob'ev, A.K. Zvezdin, D. Viehland, Phase Transitions 79 (2006) 1019–1042, https://doi.org/10.1080/01411590601067235.

[15] A.V. Pashchenko, N.A. Liedienov, Q. Li, D.D. Tatarchuk, V.A. Turchenko, I. I. Makoed, V.Ya Sycheva, A.V. Voznyak, V.P. Kladko, A.I. Gudimenko, Y. V. Didenko, A.T. Kozakov, G.G. Levchenko, J. Magn. Magn Mater. 483 (2019) 100–113, https://doi.org/10.1016/j.jmmm.2019.03.095.

[16] N.A. Liedienov, A.V. Pashchenko, V.A. Turchenko, V.Ya Sycheva, A.V. Voznyak, V. P. Kladko, A.I. Gudimenko, D.D. Tatarchuk, YuV. Didenko, I.V. Fesych, I.I. Makoed, A.T. Kozakov, G.G. Levchenko, Ceram. Int. 45 (2019) 14873–14879, https://doi.org/10.1016/j.ceramint.2019.04.220.

[17] M. Valant, A.-K. Axelsson, N. Alford, Chem. Mater. 19 (2007) 5431–5436.

[18] H.Y. Dai, Z.P. Chen, T. Li, R.Z. Xue, J. Chen, J. Supercond. Nov. Magnetism 26 (2013) 3125–3132, https://doi.org/10.1007/s10948-013-2130-7.

[19] Qing-Hui Jiang, Ce-Wen Nan, Zhi-Jian Shen, J. Am. Ceram. Soc. 89 (2006) 2123–2127, https://doi.org/10.1111/j.1551-2916.2006.01062.x.

[20] R.M. German, P. Suri, S.J. Park, J. Mater. Sci. 44 (2009) 1–39, https://doi.org/10.1007/s10853-008-3008-0.

[21] C.R. Hubbard, R.L. Snyder, Powder Diffr. 3 (1988) 74–77.

[22] Ziyu Wei, A.V. Pashchenko, N.A. Liedienov, I.V. Zatovskyi, D.S. Butenko, Quanjun Li, I.V. Fesych, V.A. Turchenko, E.E. Zubov, P.Yu Polynchuk, V.

[G.] Pogrebnyak, V.M. Poroshin, G.G. Levchenko, Phys. Chem. Chem. Phys. 22 (2020) 11817, https://doi.org/10.1039/D0CP01426E.

[23] D.D. Tatarchuk, V.I. Molchanov, V.M. Pashkov, A.S. Franchuk, Microwave Dielectric Measurement Methods on the Base of the Composite Dielectric Resonator, 2015 IEEE 35th International Conference on Electronics and Nanotechnology ELNANO-2015, April 21-24, 2015 Kyiv, Ukraine, Kyiv : "Kyiv Polytecnic Institute", 2015, pp. 231–234, https://doi.org/10.1109/ELNANO.2015.7146880.

[24] N.B. Delfard, H. Maleki, A.M. Badizi, M. Taraz, J. Supercond. Nov. Magnetism 33 (2020) 1207–1214, https://doi.org/10.1007/s10948-019-05294-3.

[25] S. Hunpratub, P. Thongbai, T. Yamwong, R. Yimnirun, S. Maensiri, Appl. Phys. Lett. 94 (2009), 062904, https://doi.org/10.1063/1.3078825.

[26] Ch Rayssi, S.El Kossi, J. Dhahri, K. Khirouni, RSC Adv. 8 (2018) 17139–17150, https://doi.org/10.1039/C8RA00794B.

[27] A.A. Akl, I.M. El Radaf, A.S. Hassanien, Superlattice. Microst. 143 (2020), 106544, https://doi.org/10.1016/j.spmi.2020.106544.

[28] Y.V. Didenko, Y.M. Poplavko, High Frequency Dielectrics: Nature of Loss, Electronics and Nanotechnology (ELNANO-2014): Proc. of 34th Int. Sci. Conf. (April 15-18, 2014, Kyiv, Ukraine). – Kyiv, 2014, pp. 73–77, https://doi.org/10.1109/ELNANO.2014.6873966.

[29] Z. Imran, M.A. Rafiq, M. Ahmad, K. Rasool, S.S. Batool, M.M. Hasan, AIP Adv. 3 (2013), 032146, https://doi.org/10.1063/1.4799756.

[30] N.J. Joshi, G.S. Grewal, V. Shrinet, T.P. Govindan, A. Pratap, IEEE Trans. Dielectr. Electr. Insul. 19 (2012) 83–90, https://doi.org/10.1109/TDEI.2012.6148505.

[31] I.I. Makoed, N.A. Liedienov, A.V. Pashchenko, G.G. Levchenko, D.D. Tatarchuk, Y. V. Didenko, A.A. Amirov, G.S. Rimski, K.I. Yanushkevich, J. Alloys Compd. 842 (2020), 155859, https://doi.org/10.1016/j.jallcom.2020.155859.

[32] V.S. Puli, D.K. Pradhan, R. Martínez, I. Coondoo, N. Panwar, R.S. Katiyar, J. Supercond. Nov. Magnetism 25 (2012) 1109–1114, https://doi.org/10.1007/s10948-011-1376-1.

[33] F.T. Mahi, O.-H. Kwon, Liquid Phase Sintering: Ceramics, 2016, https://doi.org/10.1016/b978-0-12-803581-8.03586-4.

[34] S.-J.L. Kang, Basis of Liquid Phase Sintering, 2005, pp. 199–203, https://doi.org/10.1016/b978-075066385-4/50014-5.

[35] S.H. Lee, B. Ahn, Arch. Metall. Mater. 60 (2015) 1485–1489, https://doi.org/10.1515/amm-2015-0158.

[36] T.H. Kim, S.H. Baek, S.M. Yang, S.Y. Jang, D. Ortiz, T.K. Song, J.-S. Chung, C. B. Eom, T.W. Noh, J.-G. Yoon, Appl. Phys. Lett. 95 (2009), 262902, https://doi.org/10.1063/1.3275736.

[37] S. Prosandeev, Y. Yang, C. Paillard, L. Bellaiche, npj Computational Materials (2018) 4, https://doi.org/10.1038/s41524-018-0066-y.

[38] V.V. Lazenka, G. Zhang, J. Vanacken, I.I. Makoed, A.F. Ravinski, V. V. Moshchalkov, J. Phys. D Appl. Phys. 45 (2012), 125002, https://doi.org/10.1088/0022-3727/45/12/125002.

[39] I.M. El Radaf, H.Y.S. Al-Zahrani, A.S. Hassanien, J. Mater. Sci. Mater. Electron. 31 (2020) 8336–8348, https://doi.org/10.1007/s10854-020-03369-9.

[40] A.S. Hassanien, J. Alloys Compd. 671 (2016) 566–578, https://doi.org/10.1016/j.jallcom.2016.02.126.

[41] F. Huang, X. Lu, W. Lin, Y. Kan, J. Zhang, Q. Chen, Z. Wang, L. Li, J. Zhu, Appl. Phys. Lett. 97 (2010) 222901, https://doi.org/10.1063/1.3519986.

[42] P. Maksymovych, Yu Pu Morozovska, E.A. Eliseev, Y.-H. Chu, R. Ramesh, A. P. Baddorf, S.V. Kalinin, Nano Lett. 12 (2012) 209–213, https://doi.org/10.1021/nl203349b.

[43] T. Sluka, A.K. Tagantsev, D. Damjanovic, M. Gureev, N. Setter, Nat. Commun. 3 (2012) 748, https://doi.org/10.1038/ncomms1751.